Carbohydrate Polymers 87 (2012) 881–893

Contents lists available at SciVerse ScienceDirect

Carbohydrate Polymers

journal homepage: www.elsevier.com/locate/carbpol

New hydrogels based on symmetrical aromatic anhydrides: Synthesis, characterization and metal ion adsorption evaluation

Iman Kavianinia[a], Paul G. Plieger[a], Nadia G. Kandile[b], David R.K. Harding[a,*]

[a] Chemistry, Institute of Fundamental Sciences, Massey University, Palmerston North, New Zealand
[b] Department of Chemistry, Faculty for Women, Ain Shams University, Heliopolis, Cairo, Egypt

ARTICLE INFO

Article history:
Received 19 July 2011
Received in revised form 21 August 2011
Accepted 24 August 2011
Available online 31 August 2011

Keywords:
Removal of heavy metals
Chitosan
Crosslinking
Dianhydrides

ABSTRACT

Unsatisfactory mechanical properties, poor heat resistance, dissolution in acidic media and high swelling ratios limit using chitosan as an adsorbent in industry. In this study, we used dianhydride derivatives famous for their exceptional mechanical and thermal characteristics and low water absorption. In this study, pyromellitic dianhydride (PMDA), benzophenone-3,3′,4,4′-tetracarboxylic dianhydride (BTDA), 4,4′-oxydiphthalic dianhydride (ODPA) and 4,4′-(hexafluoroisopropylidene)diphthalic dianhydride (FDA) were utilised as crosslinking agents. Use of common crosslinking agents usually decreases the metal uptake capacity of chitosan. These novel crosslinking agents increased the metal uptake from 1.8 (ODPA/Cu^{2+}) to 7.8 (PMDA/Zn^{2+}) times. Langmuir and Freundlich adsorption models were applied to analyse the isotherms and isotherm constants. Kinetic, X-ray diffraction, pH, FTIR studies were also carried out.

1. Introduction

Every living thing on earth needs water to live. Water is such an important element in our physiology. Therefore the quality of the water must be considered as important as the quantity. As a result of industrialization and urban development, water can be polluted with hundreds of toxins and other impurities. Water pollution due to hazardous metals has been a major cause of concern as they are non-biodegradable and tend to accumulate in living organisms (Bailey, Olin, Bricka, & Adrian, 1999). Over recent years, a number of technologies have been developed for removal of toxic metal ions from wastewater (Grosse, 1986). Methods for water treatment include chemical precipitation (Meunier et al., 2006), reverse osmosis (Liu, Zhang, Meng, & Zhang, 2008), ion exchange (Alyüz & Veli, 2009), adsorption (Ucer, Uyanik, & Aygun, 2006), electrodeposition and membrane systems (Bessbousse, Rhlalou, Verchère, & Lebrun, 2008). Filtration and chemical precipitation are low-cost and effective methods for removing large quantities of metal ions quickly, however they are incapable of removing trace levels of heavy metal ions effectively. Reverse osmosis, electrodeposition and membrane systems are generally effective, but these systems are expensive, sophisticated and require a higher level of technical expertise to operate.

Use of chelation ion exchange for treatment of waste water has been gaining attention recently. Chelation ion exchange, in contrast to simple ion exchange, has the advantage of removing only toxic metal ions while harmless ions can be released into the environment (Deans & Dixon, 1992). Some of the best chelation ion-exchange materials are natural biopolymers such as cellulosics, alginates, proteins, chitin, and chitin derivatives (Bailey et al., 1999). Chitosan, a linear polysaccharide that is primarily composed of β (1 → 4) linked 2-amino-2-deoxy-D-glucopyranose units and β-(1–4) linked 2-deoxy-2-acetamino-D-glucopyranose units is a very promising natural material which is commonly found in large quantities and is renewable, biodegradable and of low cost. Chitosan can be readily derived by partial deacetylation of chitin which is obtained from the shells of insects and crustaceans, as well as the cell walls of some fungi. It is known as the second most abundant naturally occurring polysaccharide after cellulose. Chitosan's inherent characteristics such as its antimicrobial activity, biocompatibility, non-toxicity and biodegradability, permit its use in many fields of interest, such as pharmaceutical and medical applications, environmental protection, textiles, wastewater treatment, biotechnology, cosmetics, food processing and agriculture (Desai et al., 2009; Kumar, Muzzarelli, Muzzarelli, Sashiwa, & Domb, 2004; Lin, Chen, & Liu, 2009). It is also used as a sorbent for heavy metal ions because the amino and hydroxy groups on the chitosan backbone can act as binding sites for metals through both chemical and physical adsorption (Gerente, Lee, Cloirec, & McKay, 2007). One of the

* Corresponding author at: Chemistry, Turitea Campus, Palmerston North, Private Bag 11222, Palmerston North 4442, New Zealand. Tel.: +64 6 6463569099; fax: +64 6 3542140.
E-mail address: d.r.harding@massey.ac.nz (D.R.K. Harding).

0144-8617/$ – see front matter © 2011 Elsevier Ltd. All rights reserved.
doi:10.1016/j.carbpol.2011.08.076

serious shortcomings of chitosan, for some applications, as a sorbent is its ability to dissolve in acidic media due to presence of amino groups (Crini, 2006). In order to improve the mechanical strength, increase the chemical stability and reduce matrix solubility at all pH, chemical and physical modifications have been used for crosslinking or insertion of new functional groups (Kandile, Mohamed, Zaky, Nasr, & Abdel-Bary, 2009; Shantha & Harding, 2002). Although the stability of cross-linked chitosan has been improved, modification procedures decrease the number of adsorption sites, consequently metal uptake decreases significantly (Chen, Liu, & Chen, 2008; Varma, Deshpande, & Kennedy, 2004; Wan Ngah, Endud, & Mayanar, 2002).

To date, the most common crosslinkers used with chitosan are glutaraldehyde or ethylene glycol diglycidyl ether. However they are not the ideal preference due to their physiological toxicity (Berger et al., 2004). Crosslinking chitosan with glutaraldehyde leads to dramatically decreased sorption properties due to decreased concentrations of complexation sites available for sorption. Wan Ngah et al. studied the removal of copper from water by modified chitosans crosslinked with three common crosslinking agents (Wan Ngah et al., 2002). Copper uptake dropped from 80.71 mg/g to 59.67 mg/g with glutaraldehyde–chitosan, to 62.47 mg/g with epichlorohydrin–chitosan and to 45.62 mg/g with ethylene glycol diglycidyl ether–chitosan. Another study by Webster et al. showed glutaraldehyde–chitosan metal uptake reductions from 20 to 80%.

The aim of this study was to improve the chemical stability of the overall matrix while overcoming the seemingly accepted decrease in metal binding capacity for the crosslinked matrix. The development of high performance, high temperature copolymers began in the late 1950s primarily to satisfy the needs of the aerospace and electronic industries (Hergenrother, 2003). Aromatic polyimides, in general, are comprised of five-membered heterocyclic imide rings. This polyimide approach was first reported by Bogert and Renshaw in 1908(Bogert & Renshaw, 1908). Polyimides have received much attention for their excellent characteristics including thermal stability, chemical resistance, excellent electrical properties, high glass transition temperature, high modulus and mechanical integrity (So, Cho, & Sahoo, 2007). These properties are influenced by the nature of moiety originating from the aromatic dianhydride (Majumdar & Biswas, 1990).

Given these copolymer enhancing properties, we chose to study the properties of two dianhydrides of pyromellitic dianhydride (PMDA) and benzophenone-3,3′,4,4′-tetracarboxylic dianhydride (BTDA) copolymerised with chitosan. In this paper, we report the first stage of our study which was to study the metal binding capabilities of these new copolymers. The initial quest was to evaluate (a) whether the dianhydride component would bind to metals, (b) evaluate any metal binding capability relative to unmodified chitosan, (c) whether the dianhydride component would to bind significant amounts of metal ions by itself and (d) extend the study if necessary, to the classic glutaraldehyde plus metal binding ligand scenario. In our study, we used PMDA and BTDA which are cheaper than glutaraldehyde and famous for their high thermal stability and oxidative stability. They also have excellent mechanical and electrical properties (Hu et al., 2010; Sroog et al., 1965; Tong, Li, Xie, & Ding, 2000). In our case the dianhydride would replace the glutaraldehyde. The more expensive ODPA and FDA were also included in this study to establish whether or not minor alterations to the two basic aromatic dianhydrides would have an effect on metal uptake.

The study showed that these new hydrogels increased the metal uptake capacity of chitosan significantly in contrast to common crosslinking agents. It was a pleasant surprise that this study revealed that the capacity for Zn^{2+} using Cts-PMDA was 7.8 times greater than unmodified chitosan. Mn^{2+} with Cts-PMDA increased 5 times, 3.3 times for Co^{2+} with Cts-ODPA, Ni^{2+} with Cts-ODPA 3.5 times, Cu^{2+} with Cts-ODPA 1.8, 7.2 times for Cr^{3+} with Cts-BTDA and for Fe^{2+} with Cts-ODPA the increase was 2.4 times greater. In other words, not only do we see a variation in the metal ion capacity for each hydrogel, we have achieved selectivity between the four hydrogels.

The outcome of this study points to these new hydrogels opening up a new area of research for the removal of hazardous material from waste water, namely custom designed metal binding crosslinking agents as opposed to hydrogels with neutral crosslinkers and metal binding ligands attached.

The following physiochemical parameters were also investigated: reaction time, pH, and initial metal ion concentration. The range of metals studied included the seven di- and trivalent first row transition metals: chromium, manganese, iron, cobalt, nickel, copper and zinc. To predict the nature of the adsorption process, the non-linear Langmuir and Freundlich isotherms were investigated to determine the best fit for predicting the nature of the adsorption process from equilibrium adsorption data. The mechanism of metal ion adsorption was also investigated using kinetic models.

2. Experimental

2.1. Materials

High molecular weight chitosan (Cts), pyromellitic dianhydride (PMDA), benzophenone-3,3′,4,4′-tetracarboxylic dianhydride (BTDA), 4,4′-oxydiphthalic dianhydride (ODPA) and 4,4′-(hexafluoroisopropylidene)diphthalic anhydride (FDA) were obtained from Sigma–Aldrich, New Zealand. Manganese chloride $MnCl_2{\cdot}4H_2O$ and chromium (III) chloride $CrCl_3{\cdot}6H_2O$ were supplied by Merck, New Zealand. Copper (II) sulfate $CuSO_4{\cdot}5H_2O$, cobalt (II) chloride $CoCl_2{\cdot}6H_2O$, zinc sulfate $ZnSO_4{\cdot}7H_2O$, nickel chloride $NiCl_2{\cdot}6H_2O$ and ferrous sulfate $FeSO_4{\cdot}7H_2O$ were obtained from May and Baker, Australia.

2.2. Chitosan degree of deacetylation

The percentage of free amine groups on the chitosan was determined by elemental analysis (Kasaai, Arul, & Charlet, 2000) using the following equation:

$$DD = \left(1 - \frac{(C/N) - 5.145}{6.186 - 5.145}\right) \times 100 \quad (1)$$

where 5.145 is related to completely *N*-deacetylated chitosan ($C_6H_{11}O_4N$ repeat unit) and 6.861 is the fully *N*-acetylated polymer ($C_8H_{13}O_5N$ repeat unit).

2.3. Preparation of hydrogels

Chitosan 0.5 g (0.0031 mol of glucosamine residues, 0.0015 mol [NH_2] calculated from the degree of deacetylation (DD) at 48.6%) was dispersed in 15 ml glacial acetic acid (100%) and shaken well for 1 h then added to the anhydride derivative dissolved in DMF (50 ml). The dianhydrides used were PMDA 0.0114 mol (0.0228 mol anhydride), BTDA 0.0077 mol (0.0154 mol anhydride), FDA 0.0056 mol (0.0112 mol anhydride), OPDA 0.0080 mol (0.016 mol anhydride). The mixture was heated at 130 °C for 24 h. The crosslinked hydrogels formed, as shown in Fig. 1a–d, were cooled. The precipitate was filtered off, washed with DMF, methanol, 0.1 mol L^{-1} NaOH and deionized water until the wash solution was neutral and then dried in vacuum.

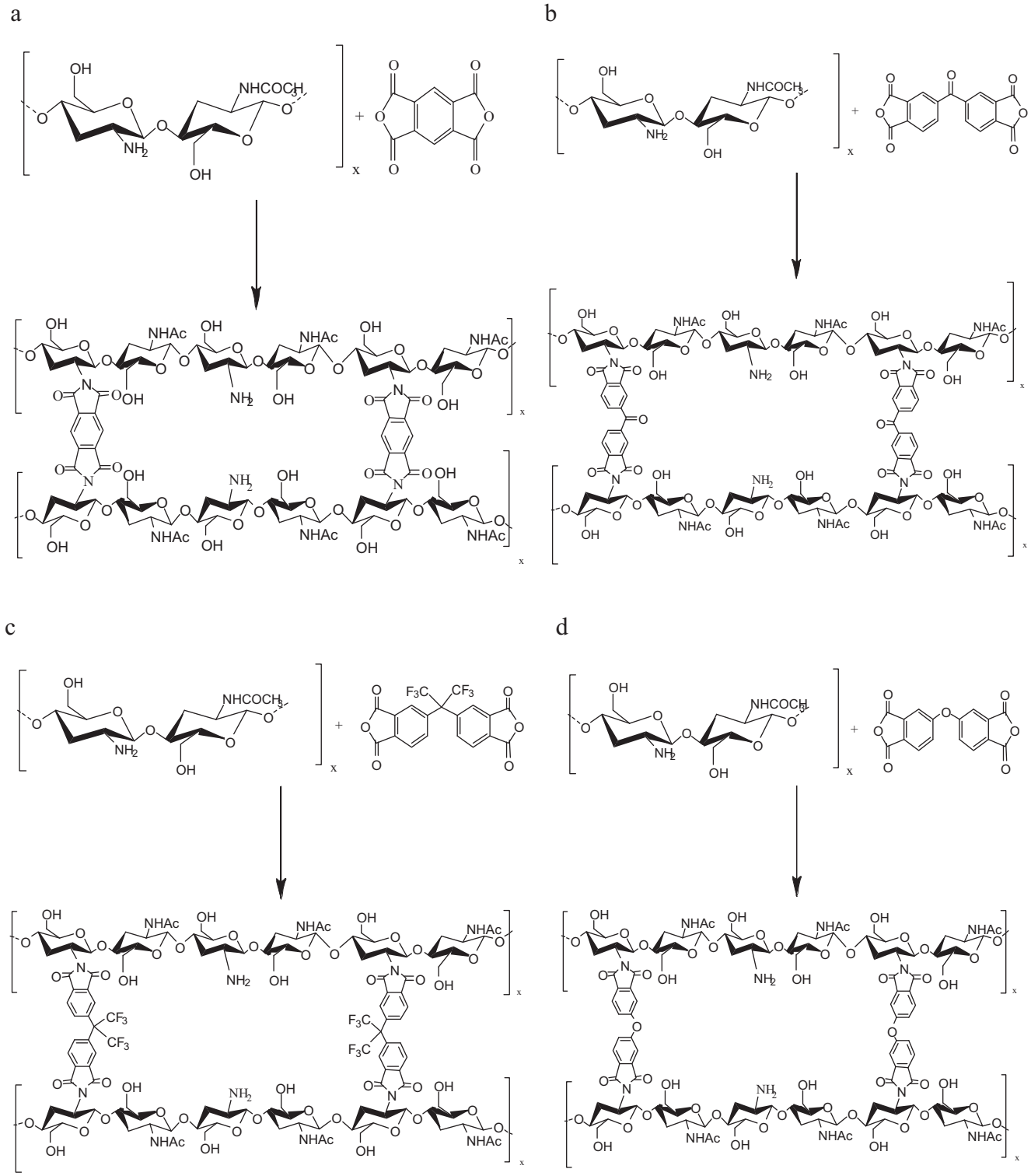

Fig. 1. Schematic representation of (a) Cts-PMDA, (b) Cts-BTDA, (c) CtS-FDA and (d) Cts-ODPA.

2.4. Characterizations of the hydrogels

2.4.1. FTIR

The FTIR spectra of the chitosan derivatives were recorded as KBr discs with a Nicolet 5700 FTIR spectrometer in the range of 400–4000 cm^{-1}.

2.4.2. Elemental analysis

Elemental analysis was performed using a Carlo Erba Elemental Analyser EA 1108 using a flash combustion technique. The analyses were carried out at the Campbell Microanalytical Laboratory, Otago University, Dunedin, New Zealand.

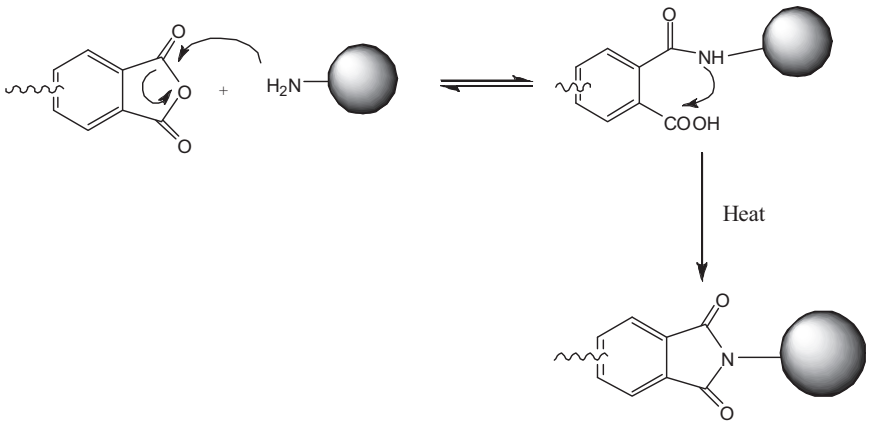

Fig. 2. Generalized reaction mechanism of aromatic imide formation.

2.4.3. Dissolution testing of chitosan and cross-linked chitosan

The chitosan and crosslinked chitosan particles were tested with regard to their solubility in each 15 mL of 5% (v/v) acetic acid, dimethylformamide, methanol, distilled water and 0.1 M sodium hydroxide solution by adding 0.1 g of chitosan and each hydrogel to each solvent for a period of 24 h with stirring.

2.4.4. X-ray diffraction analysis

The X-ray diffraction patterns were recorded on a Rigaku RAxisIV++ image-plate detector. An Axco PX70 capillary optic was used to monochromate and focus the Cu Kα radiation produced by a Rigaku MM007 micro-focus rotating-anode generator. Data were collected and analysed using Crystal Clear.

2.5. Adsorption experiments

Metal ion stock solutions (1000 ppm) were prepared in order to investigate the effect that different parameters such as pH, agitation time and heavy metal concentration had on adsorption. The stock solutions were then diluted to give a standard solution of 10 ppm. Then 50 ml aliquots of these standard solutions were placed in 50 ml volumetric flasks containing 0.010 g of chitosan or cross-linked chitosan. The flasks were agitated on a mechanical shaker at 100 rpm for a known period of time at room temperature. After filtration, the concentration of metal ions in solution was analysed using an atomic absorption spectrophotometer (GBC 903).

The optimal pH values for adsorption of metal ions were studied in the pH range of 2–6. The pH of the initial solution was adjusted by means of 0.1 M HCl or 0.1 M NaOH. Chitosan and cross-linked chitosan were equilibrated at the particular pH for about 60 min and at an initial concentration of 10 ppm.

The isotherm studies were conducted with a constant adsorbent weight (0.010 g) at optimum conditions while varying the concentration of metals ions in the range of 0–10 ppm. The extent of adsorption was calculated based on the differences in the metal ion concentration in the aqueous solution before and after adsorption, according to the following equation using Cu(II) as an example:

$$\text{Adsorption capacity } (X) = \frac{(C_0 - C_e)V}{W} \quad (2)$$

where C_0 is the initial Cu(II) concentration (ppm), C_e is the final, equilibrium Cu(II) concentration (ppm), V is the volume of Cu(II) solution (L) and W is the weight of the chitosan or cross-linked chitosan (g).

Adsorption kinetics were determined in volumetric flasks shaking at 100 rpm containing 0.010 g chitosan or crosslinked chitosan and 50 mL of metal ion solution (initial concentration 10 ppm, pH 6.0) at room temperature. During the kinetic experiments, aliquots were withdrawn at fixed time intervals, and the concentration of metal ions in solution was measured.

3. Results and discussion

3.1. Preparation of hydrogels

The imidization reaction mechanism involves the nucleophilic attack of the amino group of the chitosan on the carbonyl carbon of the anhydride group. This equilibrium reaction (Fig. 2) involves opening of the anhydride ring to form an amic acid intermediate. However, the following reaction to form the imide has a rate constant of several orders of magnitude larger than the reverse reaction (Lavrov, Ardashnikov, Kardash, & Pravednikov, 1977). Dipolar aprotic solvents, in this study DMF, prevent dissociation of the carboxyl proton, which can reverse the reaction through hydrogen bonding with the carboxyl group. The amide acid formation is exothermic (Mittal & Ghosh, 1996). Therefore the cyclization of o-carboxyamide intermediate through nucleophilic attack of the amide nitrogen on the acid carbonyl carbon with elimination of water can be readily attained by thermal imidization.

The degree of substitution (DS) was calculated on the basis of the percentage of nitrogen in the product by the following equation (Jan iauskait & Makuška, 2008):

$$\text{DS} = \frac{N - 6.61}{(686/(143 + M) + 392/(185 + M)) - 6.61} \quad (3)$$

where N is the percentage of nitrogen content shown in Table 1, and M is the molecular weight of dianhydride.

3.2. Degree of deacetylation of chitosan

The presence of the free amine groups on the chitosan backbone increases the potential for interactions with metal ions to a greater extent than the acetamide groups do (Monteiro, 1999). Therefore, the degree of deacetylation is a principal feature of chitosan that may influence its sorption properties.

The degree of deacetylation of the chitosan used in this study was 48.6% which is generally lower than other chitosans used

Table 1
CHN analysis of chitosan and crosslinked chitosan.

Percentage	Chitosan	Cts-PMDA	Cts-BTDA	Cts-FDA	Cts-ODPA
C	44.47	45.59	50.93	45.64	48.45
H	6.78	4.04	4.21	4.41	4.76
N	7.83	4.33	3.76	4.63	4.81
DS (%)	–	60	65	41	41

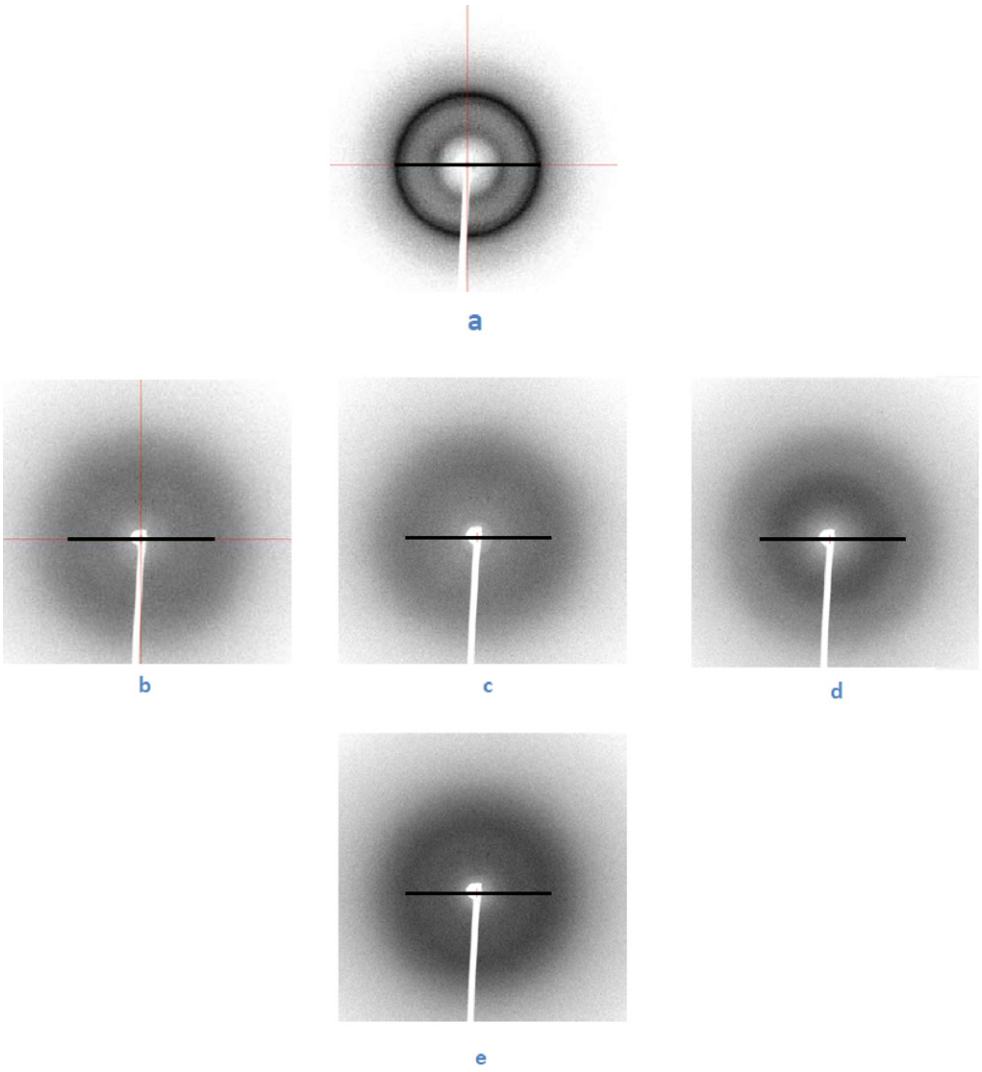

Fig. 3. 2D-XRD of (a) Cts, (b) Cts-PMDA, (c) Cts-BTDA, (d) CtS-FDA and (e) Cts-ODPA. The reference bar has length corresponding to the high-angle feature of unmodified chitosan.

in metal uptake studies (Repo, Warchol, Kurniawan, & Sillanpää, 2010). This level of deacetylation of the chitosan used in this study points to reasonable potential for biodegradation. The higher the degree of deacetylation, the more resistant chitosan becomes to enzyme decomposition, e.g. lysozyme (Kurita, Kaji, Mori, & Nishiyama, 2000).

3.3. Elemental analysis

The carbon, hydrogen and nitrogen elemental analyses for chitosan and for all modified polymers were determined by CHN analysis and these results are summarized in Table 1. It was noted that modification of chitosan decreased the percentage of nitrogen. This is due to the cross-linking agents reacting with the $-NH_2$ groups and the addition the dianhydride derivatives increasing the amount of carbon, oxygen and hydrogen in the hydrogel relative to nitrogen.

3.4. X-ray diffraction analysis

2D-XRD patterns of chitosan and its derivatives are shown in Fig. 3. The diffractogram of chitosan, Fig. 3a, shows two main crystalline peaks at 2θ values of 9.60°, and 19.28°, generally assigned to weak chain–chain ordering of the chitosan chains, in addition to several weak crystalline peaks in agreement with the characteristic diffractogram of the unmodified chitosan (Kolhe & Kannan, 2003; Nunthanid, Puttipipatkhachorn, Yamamoto, & Peck, 2001). This diffraction pattern shows the partially crystalline structure of chitosan. These diffraction signals at $2\theta = 9.6°$ ($d \sim 9.2$ Å) and 19.3° ($d \sim 4.6$ Å) were not observed in the XRD patterns Fig. 3b–e, which indicates that the chemical crosslinking between chitosan and various dianhydride derivatives destroys the crystallinity of chitosan and increases the amorphous volume in the modified chitosan hydrogel. The reduction in crystallinity of chitosan after modification is evidence for irregular packing of chitosan subunits as a result of the crosslinking (Monteiro & Airoldi, 1999). The substitution of amino groups by anhydride derivatives causes a reduction of the strong hydrogen bonding that is found in the unmodified chitosan.

Samples Cts-PMDA (Fig. 3b), Cts-BTDA (Fig. 3c) and Cts-ODPA (Fig. 3e) show a single very broad weak band at ~19° indicating vestiges of the parent chitosan structure. On the other hand, the diffractogram for CtS-FDA (Fig. 3d) is distinctly different to samples Cts-PMDA, Cts-BTDA and Cts-ODPA. The diffuse maximum is shifted to ~12°. The weak low-angle diffraction feature at ~9.5° is generally assigned to weak lengthwise ordering between chitosan subunits. The weak feature at ~12° is assigned to an increase in separation between chains caused by this rigid linker.

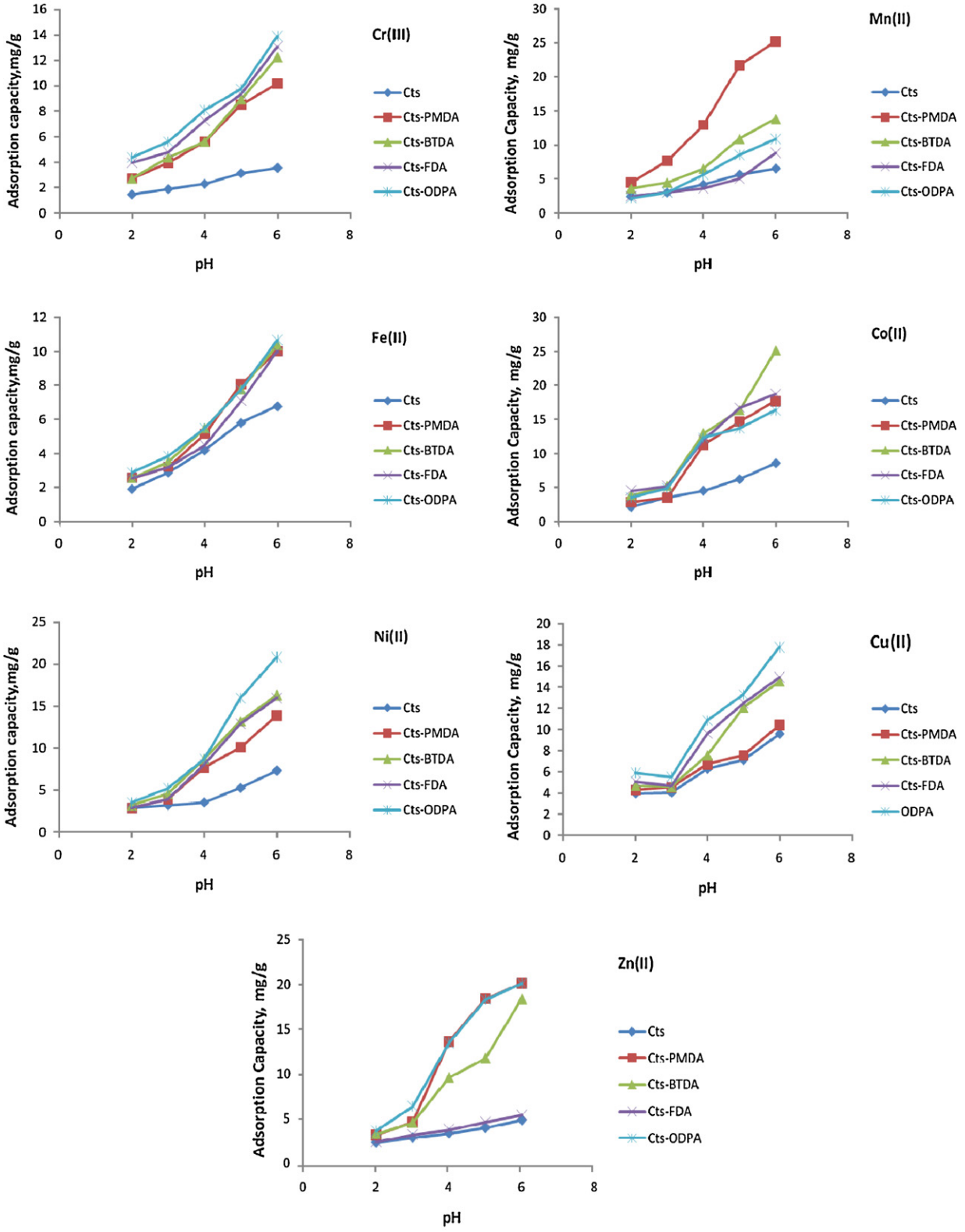

Fig. 4. Effect of pH on the metal adsorption on chitosan and crosslinked chitosans.

3.5. Solubility test of chitosan and crosslinked chitosan

It has been well known that the substantial hydrophilicity of chitosan due to its primary amino group makes it readily soluble in dilute organic acids and hence readily allows the preparation of hydrogels in water (Hsien & Rorrer, 1995). The end result is that crosslinking chitosan instils chemical stability in acidic media, permitting the resulting hydrogel to be used for the removal of chemical pollutants from wastewaters in acidic solution.

The solubility of the anhydride crosslinked chitosan derivatives was checked in various solvents. It is shown in Table 2 that after

Table 2
Dissolution test of chitosan and crosslinked chitosan.

Powder	Solubility effect				
	Acetic acid	0.1 M NaOH	DMF	Methanol	Distilled water
Chitosan	Soluble	Insoluble	Insoluble	Insoluble	Insoluble
Cts-PMDA	Insoluble	Insoluble	Insoluble	Insoluble	Insoluble
Cts-BTDA	Insoluble	Insoluble	Insoluble	Insoluble	Insoluble
Cts-FDA	Insoluble	Insoluble	Insoluble	Insoluble	Insoluble
Cts-ODPA	Insoluble	Insoluble	Insoluble	Insoluble	Insoluble

crosslinking, the crosslinked chitosan was found to be insoluble in acidic and alkaline medium as well as methanol, dimethylformamide and distilled water.

3.6. Effect of pH

Fig. 4 shows the effect of acidity on the adsorption of metal ions by chitosan and cross-linked chitosan. It can be seen that adsorption increases with increasing pH of the solution. Therefore, essentially competition between hydrogen ions and metal cations diminishes the metal chelating ability of these chitosans. At higher pH (>6) values, precipitation of metal hydroxide occurs simultaneously with the adsorption of metal ions. Therefore, pH 6.0 was chosen for the adsorption of metal ions in this study to avoid the formation of metal hydroxide.

3.7. IR analysis of hydrogels

In this study, FTIR analysis was employed to investigate the characteristic chemical structure of the chitosan and the chitosan derivatives (Cts-PMDA, Cts-BTDA, Cts-FDA, Cts-ODPA). The FTIR results for the crosslinked chitosans and unmodified chitosan are shown in Fig. 5. The major peaks for the Cts in Fig. 5a can be attributed as follows: 3431.9 cm^{-1} –OH and –NH stretching vibrations, 2879.6 cm^{-1} –CH stretching vibration in –CH and $–CH_2$, 1653.5 and 1598.3 cm^{-1} amide –C=O bond of the remaining acetamido groups and N–H bending vibration of $–NH_2$ groups respectively, 1420.3 cm^{-1} can be assigned to the –NH deformation vibration in $–NH_2$, 1380.5 cm^{-1} –CH symmetric bending vibration in –CHOH, 1322 and 1155.6 cm^{-1} C–N stretching vibration, 1076.4 and 1030.7 cm^{-1} –CO stretching vibration in –COH. After modification of chitosan, the spectra (Fig. 5b–e) showed some major changes. The peak at 3431.9 cm^{-1} of Cts was slightly broadened and shifted to 3475.2 cm^{-1}, 3420.5 cm^{-1}, 3421.1 cm^{-1}, 3427 cm^{-1} for Cts-PMDA, Cts-BTDA, Cts-FDA, Cts-ODPA respectively. The reduction in the intensity and wave numbers related to –NH bending and deformation vibrations indicate that the primary amino groups were involved in the cross linking process.

The characteristic bands of symmetrical C=O stretching and unsymmetrical C=O stretching of the imide group were clearly visible at 1721 cm^{-1} and 1778 cm^{-1}, respectively for Cts-PMDA, 1718 cm^{-1} and 1778 cm^{-1} for Cts-BTDA, 1717.9 cm^{-1} and 1780.2 cm^{-1} for Cts-FDA and 1717.5 cm^{-1} and 1773.5 cm^{-1} for Cts-ODPA. Peaks related to imide ring deformation were at 749 cm^{-1}, 733 cm^{-1}, 753 cm^{-1}, 742 cm^{-1} for Cts-PMDA, Cts-BTDA, Cts-FDA, Cts-ODPA, respectively.

3.8. Adsorption isotherms

Adsorption isotherms describe how adsorbates interact with adsorbents and so are critical in optimising the use of adsorbents (Ng, Cheung, & McKay, 2002). The quantity of adsorbate that can be taken up by a particular adsorbent is a function of both the

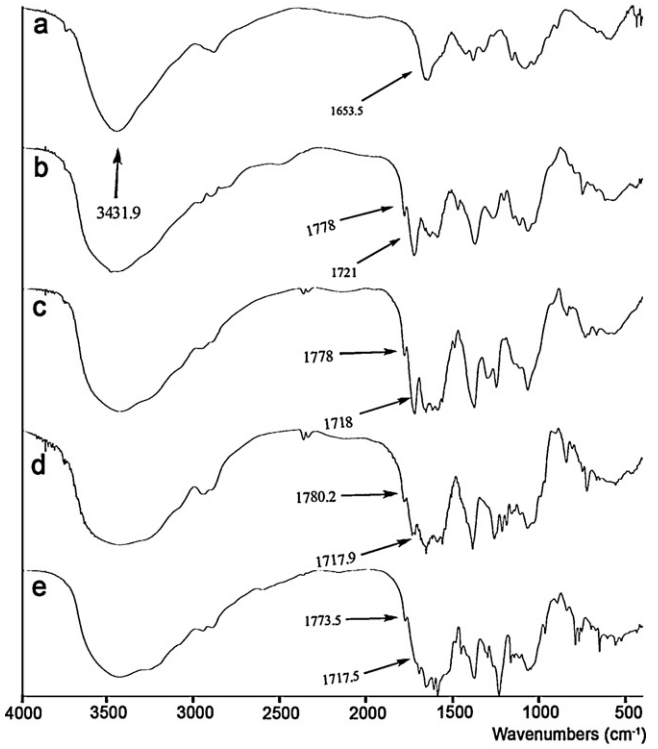

Fig. 5. FTIR spectra of (a) Cts, (b) Cts-PMDA, (c) Cts-BTDA, (d) CtS-FDA and (e) Cts-ODPA.

characteristics and concentration of adsorbate and the temperature. The correlation of equilibrium data by either theoretical or empirical equations is essential to the practical design and operation of adsorption systems. In order to optimise the design of a sorption system to remove metal ions from effluents, it is important to establish the most appropriate correlation for the equilibrium curves. Two equations that are often used to describe the experimental isotherm data was developed by two scientists Langmuir and Freundlich (Metcalf, Eddy, & Tchobanoglous, 1991).

3.8.1. Langmuir isotherm

Langmuir (1918) proposed a theory to describe the adsorption of gas molecules onto metal surfaces. The Langmuir adsorption isotherm has found successful application to many other real sorption processes involving monolayer adsorption. Langmuir's model of adsorption depends on the assumption that intermolecular forces decrease rapidly with distance and consequently predicts the existence of monolayer coverage of the adsorbate at the outer surface of the adsorbent. The isotherm equation further assumes that adsorption takes place at specific homogeneous sites within the adsorbent. It is then assumed that once a dye molecule occupies a site, no further adsorption can take place at that site. Moreover, the Langmuir equation is based on the assumption of a structurally homogeneous adsorbent where all sorption sites are identical and energetically equivalent. Theoretically, the sorbent has a finite capacity for the sorbate. Therefore, a saturation value is reached beyond which no further sorption can take place. The saturated or monolayer (as Cts $\rightarrow \infty$) capacity can be represented by the expression:

$$q_e = \frac{K_L C_e}{1 + a_L C_e} \quad (4)$$

where q_e is solid phase sorbate concentration at equilibrium (mg/g), C_e is aqueous phase sorbate concentration at equilibrium (ppm), K_L is Langmuir isotherm constant (ml/g), a_L is Langmuir isotherm constant (ml/mg).

Table 3
Langmuir and Freundlich parameters data for metal ions adsorption onto chitosan and crosslinked chitosan.

Hydrogels	Metal ions	Langmuir constants			Freundlich constants		
		Q_0 (mg/g)	a_L (ml/mg)	R^2	$1/n$	K_F (mg/g)	R^2
Chitosan	Cr^{3+}	7.662	1.837	0.996	0.393	1.107	0.9766
	Mn^{2+}	14.619	0.986	0.9959	0.247	7.700	0.9668
	Fe^{2+}	16.260	0.538	0.9975	0.144	25.142	0.9364
	Co^{2+}	18.975	0.770	0.9969	0.234	18.967	0.897
	Ni^{2+}	14.992	0.577	0.9972	0.145	10.192	0.9826
	Cu^{2+}	30.030	1.11	0.9982	0.302	14.034	0.9672
	Zn^{2+}	10.952	1.314	0.9984	0.337	5.671	0.953
Cts-PMDA	Cr^{3+}	36.231	0.333	0.9999	0.127	11.167	0.9216
	Mn^{2+}	67.114	0.483	0.9965	0.120	48.741	0.9663
	Fe^{2+}	38.022	0.505	0.9998	0.170	11.176	0.941
	Co^{2+}	55.555	0.233	0.9999	0.090	44.750	0.9315
	Ni^{2+}	46.948	0.262	0.9999	0.112	36.249	0.8795
	Cu^{2+}	48.780	0.512	0.9988	0.178	31.571	0.905
	Zn^{2+}	76.923	0.261	0.9994	0.084	62.531	0.8552
Cts-BTDA	Cr^{3+}	47.846	0.296	0.9998	0.138	11.161	0.7894
	Mn^{2+}	49.019	0.411	0.9998	0.160	33.635	0.957
	Fe^{2+}	32.894	0.421	0.9992	0.134	23.566	0.9672
	Co^{2+}	52.910	0.179	0.9998	0.104	42.237	0.6554
	Ni^{2+}	50.761	0.309	0.9998	0.115	38.485	0.9202
	Cu^{2+}	42.372	0.457	0.9988	0.150	29.322	0.957
	Zn^{2+}	54.945	0.263	0.9996	0.086	44.299	0.964
Cts-FDA	Cr^{3+}	36.764	0.043	0.9984	0.113	12.628	0.9933
	Mn^{2+}	23.255	0.751	0.9991	0.244	12.8913	0.8636
	Fe^{2+}	26.525	0.464	0.9991	0.157	18.080	0.9144
	Co^{2+}	37.313	0.473	0.9979	0.122	23.033	0.9836
	Ni^{2+}	41.841	0.523	0.9975	0.147	28.793	0.9169
	Cu^{2+}	41.332	0.545	0.9975	0.152	27.931	0.9052
	Zn^{2+}	20.790	0.781	0.9991	0.225	11.819	0.9706
Cts-ODPA	Cr^{3+}	46.728	0.565	0.9982	0.158	9.4518	0.9799
	Mn^{2+}	31.948	0.792	0.9989	0.256	17.210	0.9108
	Fe^{2+}	39.215	0.301	0.9991	0.104	30.241	0.8895
	Co^{2+}	60.240	0.307	0.9996	0.088	47.907	0.9887
	Ni^{2+}	51.813	0.290	0.9993	0.090	41.295	0.9394
	Cu^{2+}	51.282	0.482	0.9993	0.155	34.833	0.9678
	Zn^{2+}	72.463	0.282	0.9999	0.128	54.062	0.8789

Therefore, a plot of C_e/q_e versus C_e gives a straight line of slope a_L/K_L and the intercept $1/K_L$, where K_L/a_L gives the theoretical monolayer saturation capacity, Q_0. The Langmuir equation is applicable to homogeneous sorption where the sorption of each sorbate molecule onto the surface has equal sorption activation energy. The Langmuir equation obeys Henry's Law at low concentration; when the concentration is very low, $a_L C_e$ is far smaller than unity, it implies $q_e = K_L C_e$, hence, it is analogous to Henry's Law. Therefore, a linear expression of Langmuir equation is:

$$\frac{C_e}{q_e} = \frac{1}{K_L} + \frac{a_L}{K_L} C_e \tag{5}$$

3.8.2. Freundlich isotherm

The widely used empirical Freundlich equation can be applied to adsorption at heterogeneous surfaces and situations that involve multilayer sorption. The Freundlich equation is commonly expressed by Eq. (5):

$$q_e = K_F C_e^{1/n} \tag{6}$$

where q_e is the amount of metal ion adsorbed per unit weight of the sorbent (mg/g), C_e is the equilibrium concentration of the solute in the blank solution (ppm), K_F is the Freundlich constant (mg/g), and $1/n$ is the heterogeneity factor. A linear form of the Freundlich expression can be obtained by taking logarithms of Eq. (5).

$$\ln q_e = \ln K_F + \left(\frac{1}{n}\right) \ln\ C_e \tag{7}$$

Therefore, a plot of $\ln q_e$ versus $\ln C_e$ enables the constant K_F and the exponent $1/n$ to be determined. This isotherm is another form of the Langmuir approach for adsorption on an "amorphous" surface. The amount of adsorbed material is the summation of adsorption on all sites. The Freundlich isotherm is derived by assuming an exponential decay energy distribution function inserted into the Langmuir equation. It describes reversible adsorption and is not restricted to the formation of the monolayer. The Freundlich equation predicts that the metal ion concentrations on the adsorbent will increase so long as there is an increased in the metal ion concentration in the liquid. A smaller $1/n$ value indicates a more heterogeneous surface whereas a value closer to or equal to one indicates the adsorbent has relatively more homogeneous binding sites. The n value is a constant which represents adsorption intensity (Trimukhe & Varma, 2008).

The isotherm parameters for the adsorption of the metal ions in this study are shown in Table 3. Based on the coefficients obtained (Table 3), it can be concluded that the Langmuir equation provides the best fit for metal adsorption on the chitosan and the crosslinked chitosans in the concentration range studied (correlation coefficient was found to be $R > 0.99$).

3.8.3. Separation factor

The basic characteristics of the Langmuir isotherm can be expressed in terms of the dimensionless constant separation factor for equilibrium parameter, R_L (McKay, El Geundi, & Nassar, 1987), defined as follows:

$$R_L = \frac{1}{1 + a_L C_0} \tag{8}$$

Table 4
R_L values based on the Langmuir equation.

Metal ions	R_L values				
	Cts	Cts-PMDA	Cts-BTDA	Cts-FDA	Cts-ODPA
Cr^{3+}	0.213	0.600	0.628	0.920	0.469
Mn^{2+}	0.336	0.508	0.548	0.399	0.386
Fe^{2+}	0.481	0.497	0.542	0.518	0.624
Co^{2+}	0.393	0.682	0.736	0.513	0.619
Ni^{2+}	0.464	0.656	0.618	0.488	0.632
Cu^{2+}	0.310	0.494	0.522	0.478	0.509
Zn^{2+}	0.275	0.657	0.655	0.390	0.639

where C_0 is the highest initial solute concentration in the liquid phase (ppm), a_L is Langmuir adsorption equilibrium constant (ml/mg). The R_L value implies that adsorption is either unfavourable ($R_L > 1$), linear ($R_L = 1$), favourable ($0 < R_L < 1$), or irreversible ($R_L = 0$).

The values of R_L calculated for chitosan and cross-linked chitosan are given in Table 4. The R_L values show that favourable adsorption of metal ions onto chitosan and the cross-linked chitosans takes place. Therefore chitosan and the cross-linked chitosans are favourable adsorbents.

3.9. Kinetic study

In order to investigate the mechanism of sorption and potential rate controlling steps such as mass transport and chemical reaction processes, kinetic models were employed. A pseudo first-order model and a pseudo second-order model were used to interpret the sorption kinetics (Cheung, Ng, & Mckay, 2003).

3.9.1. The pseudo first-order model

Fig. 6 shows the relationship between the agitation time and adsorption capacities of chitosan and modified chitosan for metal ions. As can be seen, the adsorption capacity increases rapidly in the early stages of the reaction and obtains equilibrium at approximately 14 h for Cr^{3+}, Mn^{2+}, Fe^{2+}, Co^{2+}, Ni^{2+} and about 24 h for $Cu^{2+}$and Zn^{2+}. To examine the controlling mechanism of adsorption processes such as mass transfer and chemical reactions, Pseudo first-order model, pseudo second-order model have been used to interpret sorption kinetics.The first-order rate equation of Lagergren (1898) is one of the most widely used for the adsorption of a solute from a liquid solution. It may be represented as follows:

$$\frac{dq_t}{dt} = k_1(q_e - q_t) \tag{9}$$

where q_t is amount of metal adsorbed at any time (mg/g), q_e is amount of metal adsorbed at equilibrium time (mg/g) and k_1 is pseudo first-order rate constant (min^{-1}).

After definite integration by applying the initial conditions $q_t = 0$ at $t = 0$ and $q_t = q_t$ at $t = t$, Eq. (8) becomes

$$\text{Log}\ \frac{q_e}{q_e - q_t} = \frac{(k_1 t)}{2.303} \tag{10}$$

Eq. (9) can be rearranged to obtain a linear form:

$$\text{Log}\ (q_e - q_t) = \log q_e - \left(\frac{k_1}{2.303}\right) t \tag{11}$$

Table 5
Kinetic parameters for metal ions adsorption onto chitosan and crosslinked chitosan.

Hydrogels	Metal ions	First-order		Second-order		
		10^3 K (min^{-1})	R^2	10^4 K (g mg^{-1} min^{-1})	R^2	q
Chitosan	Cr^{3+}	4.606	0.9408	29.73	0.9853	6.901
	Mn^{2+}	4.145	0.976	9.121	0.9872	14.044
	Fe^{2+}	3.684	0.9265	8.238	0.9941	16.666
	Co^{2+}	5.987	0.9894	8.068	0.993	18.761
	Ni^{2+}	8.060	0.9867	10.93	0.9902	15.649
	Cu^{2+}	7.830	0.963	0.890	0.9919	31.446
	Zn^{2+}	11.5	0.9228	27.13	0.9964	10.395
Cts-PMDA	Cr^{3+}	5.066	0.9772	1.520	0.9776	41.332
	Mn^{2+}	6.448	0.9876	1.349	0.9944	74.074
	Fe^{2+}	5.757	0.9915	1.538	0.9782	43.478
	Co^{2+}	5.296	0.979	1.133	0.9862	62.893
	Ni^{2+}	6.448	0.9641	0.942	0.9641	56.818
	Cu^{2+}	3.454	0.9025	1.689	0.9938	53.763
	Zn^{2+}	3.224	0.9233	0.8615	0.9974	82.644
Cts-BTDA	Cr^{3+}	6.218	0.9531	0.750	0.9668	60.240
	Mn^{2+}	6.218	0.9876	1.422	0.9861	54.945
	Fe^{2+}	5.527	0.9791	2.083	0.9803	36.363
	Co^{2+}	5.757	0.9862	2.671	0.9966	55.555
	Ni^{2+}	5.987	0.9797	1.219	0.9878	57.803
	Cu^{2+}	3.454	0.9005	1.905	0.996	43.859
	Zn^{2+}	3.454	0.9246	0.979	0.9904	59.523
Cts-FDA	Cr^{3+}	5.066	0.9627	1.916	0.9717	39.840
	Mn^{2+}	4.606	0.9657	6.523	0.9947	22.988
	Fe^{2+}	5.296	0.9884	4.432	0.9902	27.322
	Co^{2+}	5.296	0.9842	4.070	0.9978	38.314
	Ni^{2+}	5.527	0.9758	2.051	0.9932	44.843
	Cu^{2+}	3.454	0.9458	1.940	0.9959	42.735
	Zn^{2+}	2.303	0.9177	3.127	0.9927	20.920
Cts-ODPA	Cr^{3+}	5.527	0.9859	1.240	0.9787	53.191
	Mn^{2+}	5.527	0.9932	2.860	0.9903	33.557
	Fe^{2+}	5.757	0.9665	2.223	0.9868	42.016
	Co^{2+}	6.448	0.992	0.936	0.9799	70.921
	Ni^{2+}	5.757	0.9857	1.803	0.9886	56.497
	Cu^{2+}	2.763	0.9507	1.6445	0.9962	52.356
	Zn^{2+}	4.145	0.9511	0.6813	0.9921	79.365

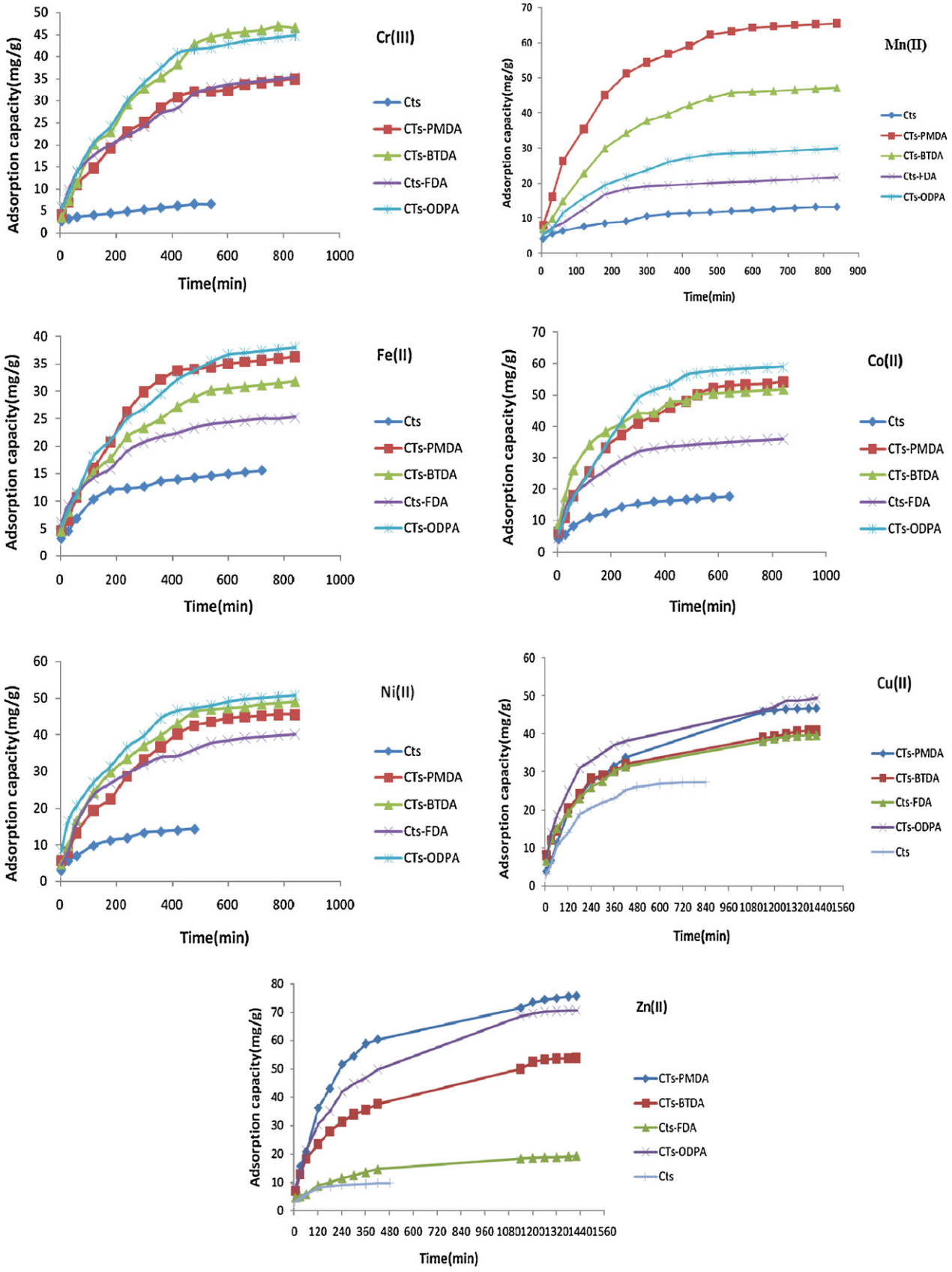

Fig. 6. Effect of agitation time on the adsorption of metal ions on chitosan and crosslinked chitosans.

Table 6
Characteristic of vibrational frequencies (cm^{-1}) of the chitosan and crosslinked chitosan.

Hydrogel	Metal	ν(OH)/ν(NH)	ν(C=O)	ν(C–N)	ν(C–O–C)	ν(C–O)
Chitosan	Cr^{3+}	3436.5 br, s	–	1321 w,1156 w	–	1094 m,1070 w
	Mn^{2+}	3366.5 br, s	–	1322.4 w,1154 w	–	1093 m,1030.9 w
	Fe^{2+}	3435.5 n, vs	–	1355.2 w,1119.9 w	–	1018 w,935.7 w
	Co^{2+}	3436.0 n, vs	–	1324.3 w,1156.7 w	–	1088.3 m,1047.7 m
	Ni^{2+}	3475.5 br, m,3291.9 br, m	–	1321 w,1154.1 w	–	1070.2 w,1024.7 w
	Cu^{2+}	3419.3 br, s	–	1320.1 w,1155.2 w	–	1094 w,1070.6 w
	Zn^{2+}	3436.6 n, vs	–	1322.7 w,1154 w	–	1116.1 w,1031.6 w
Cts-PMDA	Cr^{3+}	3418.9 br, s	1778.9 w,1717.9 s	1255.5 w,1115 w	–	1110.71 m,1061.6 m
	Mn^{2+}	3426.9 br, s	1778 w,1718 m	1246 w,1203.3 w	–	1107.7 m,1066 m
	Fe^{2+}	3439 n, s	1778.7 w,1721.9 m	1320 w,1145.6.1 w	–	1112.4 w,1052.6 w
	Co^{2+}	3389.2 br, s	1177.7 w,1722.5 m	1299 w,1147.1 w	–	1114 w,1091 w
	Ni^{2+}	3448.1 br, m	1776.7 w, 1722.9 m	1288 w,1147.2 w	–	1026 w,1010 w
	Cu^{2+}	3081.5 br	11781 w,1725.9 m	1188 w,1109.1 w	–	1114 w,1091 w
	Zn^{2+}	3434.8 n, s	1778.9 w,1718.5 m	1269 w,1147.2 w	–	1112.7 w,1063.5 w
Cts-BTDA	Cr^{3+}	3437.9 n, s	1778.8 w,1722 m	1247.1 w,1158.6 w	–	1108 w,1064.2 w
	Mn^{2+}	3418.6 br, s	1778.2 w,1721 m	1245.7 w,1154 w	–	1098 w,1064.8 w
	Fe^{2+}	3426.7 n, s	1779 w,1719.4 m	1245.6 w,1135.3 w	–	1125.5 w,1094.3 w
	Co^{2+}	3436.3 n, s	1778.4 w,1722.1 m	1245.7 w,1174.1 w	–	1098 w,1064.8 w
	Ni^{2+}	3434.9 n, s	1778.6 w,1718.7 m	1247.1 w,1143.8 w	–	1115 w,1048.3 w
	Cu^{2+}	3438.5 n, s	1772.1 w,1716.9 s	1246 w,1142.2 w	–	1117.3 w,1073.1 w
	Zn^{2+}	3438.5 n, s	1778.6 w,1719.2 m	1246.7 w,1142.2 w	–	1107.3 w,1065.2 w
Cts-FDA	Cr^{3+}	3413.7 br, s	1773.5 w,1716.6 m	1231.3 w,1152.8 w	–	1108.6 w,1063.3 w
	Mn^{2+}	3439.7 n, br	1779.4 w,1722.9 m	1214 w,1189.2 w	–	1066 w,1031 w
	Fe^{2+}	3418.2 br, s	1780.7 w,1723.7 m	1213.1 w,1188.7 w	–	1106.9 w,1066.2 w
	Co^{2+}	3385.7 n, s	1778.9 w,1722.5 m	1273.7 w,1214.8 w	–	1090.5 s,1050.3 s
	Ni^{2+}	3481.9 br, s	1773.6 w,1715.8 m	1272.1 w,1272.1 w	–	1117 w,1021.6 w
	Cu^{2+}	3428.7 br	1778.3 w,1718.5 s	1256 w,1146.9 w	–	1110.8 w,1064.4 w
	Zn^{2+}	3437.6 n, s	1780.7 w,1718.1 s	1214.4 w,1189.2 w	–	1116.1 w,1028.2 w
Cts-ODPA	Cr^{3+}	3445.3 n,s	1773.2 w,1717.6 m	1258.3 w,1188.4 w	1213.4 w	1118.2 w,1066.6 w
	Mn^{2+}	3392.7 br,s	1775.2 w,1721.3 m	1267.9 w,1122.9 w	1230.9 w	1112.2 w,1065.3 w
	Fe^{2+}	3436.1 n, s	1774.1 w,1716.3 m	1269.1 w,1220.4 w	1230.9 w	1111.6 w,1047.9 w
	Co^{2+}	3394.5 br, s	1773.8 w,1712.9 m	1274.9 w,1132.1 w	1232.2	1089.8 w,1049.7 w
	Ni^{2+}	3417 br, s	1780.2 w,1724.1 m	1258.7 w,1113.2 w	1213.7	1069.2 w,1019 w
	Cu^{2+}	3415.4 br.s	1775.4 w,1720.9 m	1266.5 w,1194.1 w	1230.5 m	1069.2 w,1049.7 w
	Zn^{2+}	3447.4 n, s	1773.1 w,1716 m	1278.2 w,1153.9 w	1236.4 w	1114.9.2 w,1019.2 w

A plot of log $(q_e - q_t)$ versus t gives a straight line for pseudo first-order kinetics, which allows computation of the sorption rate constant, k_1 (Ofomaja, Naidoo, & Modise, 2010).

3.9.2. The pseudo-second-order model

The pseudo-second-order equation based on the adsorption equilibrium capacity may be expressed as follows (Gerente et al., 2007):

$$\frac{dq_t}{dt} = k_2(q_e - q_t) \tag{12}$$

where q_t is amount of metal adsorbed at any time (mg/g), q_e is amount of metal adsorbed at equilibrium time (mg/g) and k_2 is pseudo second-order rate constant (g/mg min).

Separating the variables in Eq. (11) and applying the boundary conditions gives

$$\frac{dq_t}{(q_e - q_t)^2} = k_2(q_e - q_t) \tag{13}$$

Integrating this for the boundary conditions $t = 0$ to $t = t$ and $q_t = 0$ to $q_t = q_t$ gives:

$$\frac{1}{(q_e - q_t)} = \frac{1}{q_e} + k_2 t \tag{14}$$

or equivalently,

$$\frac{t}{q_t} = \frac{1}{k_2 q_e^2} + \frac{1}{q_t} t \tag{15}$$

It should be noted that, compared to Eq. (13), Eq. (14) has an advantage that k_2 and q_e can be obtained from the intercept and slope of the plot t/q_t vs t.

The kinetic parameters for adsorption of the seven metal ions are shown in Table 5. According to the correlation coefficient, the pseudo second-order model, in contrast to the pseudo first-order, gave the best fit for the experimental kinetic data. The calculated q_e values are close to the experimental data, indicating that chemical sorption was the rate-limiting step of the adsorption mechanism and mass transfer of the solution is not involved (Wu, Tseng, & Juang, 2001). This means that the adsorption behaviour may involve valency forces through the sharing of electrons between transition metal cations and adsorbent.

3.10. Infrared spectra of the chitosan and hydrogels after metal uptake

The spectra of chitosan and crosslinked chitosan derivatives after metal ion adsorption exhibit many alterations as listed in Table 6. The major differences are the broad band at 3419 cm^{-1}, corresponding to the stretching vibration of the NH_2 and OH groups which exhibit a change in shape and shift to lower and higher wavelengths. The respective changes in intensity and position of peaks related to N–H deformation and C–N stretching vibration suggested the interaction between metal ions with the nitrogen atoms. In addition, changes in intensity and wavelength of peaks in the region from 1000 cm^{-1} to 1200 cm^{-1} verify the complexation of the chitosan not only via the amine groups, but also through the OH groups. In this region chitosan presents bands attributed to the C–O stretching of primary and secondary alcohol of chitosan.

In the case of Cts-ODPA, the peak at 1231.5 which is related to the ether functional group showed a significant change in intensity indicating metal adsorption.

In the spectra of the modified chitosans, the peaks related to the C=O stretching in the imide groups have changed in intensity, indicating a role of the C=O imides in the interaction with metals.

4. Conclusions

The prime aim of this study was to investigate new crosslinking agents for chitosan that would have the potential for increasing the resulting hydrogel's metal ion binding capabilities beyond that of basic chitosan itself. It is well known that crosslinking procedures decrease the number of adsorption sites, consequently metal adsorption decreases significantly (Wan Ngah et al., 2002). These new hydrogels show increased metal uptake relative to unmodified chitosan. The most likely explanation being that the crosslinking agents are taking part in the metal uptake. Crosslinking has also decreased the crystallinity of un-derivatised chitosan and hence has improved the accessibility of any remaining amino and undervatised hydroxyl groups (Monteiro & Airoldi, 1999). We believe that these new hydrogels for at least some applications can be used for future research efforts instead of glutaraldehyde, perhaps the most popular crosslinking agent used in chitosan hydrogel preparations. These new chitosan derivatives are expected to not only improve the chemical stability of chitosan but also increase metal uptake ability.

To this end four dianhydride crosslinkers were investigated. In all four cases, PMDA, BTDA, FDA and ODPA, the resulting hydrogels bound all metal ions tested to a greater extent than the parent chitosan. It was revealed from this study that the maximum capacity for monolayer saturation was 75.7 mg g^{-1} Zn^{2+} by Cts-PMDA (~7.8 times greater than unmodified chitosan), 65.6 mg g^{-1} Mn^{2+} by Cts-PMDA (~5 times greater), 59.0 mg g^{-1} Co^{2+} by Cts-ODPA (~3.3 times greater), 50.8 mg g^{-1} Ni^{2+} by Cts-ODPA (~3.5 times greater), 49.4 mg g^{-1} Cu^{2+} by Cts-ODPA (~1.8 times greater), 46.5 mg g^{-1} Cr^{3+} by Cts-BTDA (~7.2 times greater) and 38.0 mg g^{-1} Fe^{2+} by Cts-ODPA (~2.4 times greater).

As mentioned above, this family of aromatic diahydrides has a reputation for strengthening polymers. Thus the second objective was to begin a move toward tougher soft gels to be used for chromatographic objectives, especially on the larger scale. In other words, a major focus is on large scale chromatographic separations of hazardous materials from water. The objective appears feasible. BTDA and PMDA in particular have a considerable track record (Sroog et al., 1965) in the world of synthetic copolymers. In short they are inexpensive reagents, they increase the strength of copolymers (Mittal, 2009; Sroog et al., 1965; Tong et al., 2000) and have known ionic conduction capabilities (Tian & Xu, 1995).

In summary chitosan crosslinked with aromatic dianhydrides has been realised to achieve an increase of metal binding over the parent chitosan. The nature of these dianhydrides bodes well for tougher cellulosic gels for use in many purifucation applications needing a gel that is fit for recycling and is biodegradable. This investigation has revealed that the four chitosan hydrogels studied were achieved by copolymerisation with symmetrical aromatic dianhydrides alone to achieve significant metal binding. In all cases, the binding was greater than that of the unmodified chitosan used in this study. Studies are now proceeding to evaluate the physical chemical properties of these hydrogels. Biodegrability is also being studied.

Acknowledgements

We would like to acknowledge and thank Professor GB Jameson, Chemistry and Biophysics, Institute of Fundamental Sciences, Massey University, Palmerston North, New Zealand, for his assistance with the interpretation of the X-ray data.

References

Alyüz, B., & Veli, S. (2009). Kinetics and equilibrium studies for the removal of nickel and zinc from aqueous solutions by ion exchange resins. *Journal of Hazardous Materials*, *167*(1–3), 482–488.
Bailey, S. E., Olin, T. J., Bricka, R. M., & Adrian, D. D. (1999). A review of potentially low-cost sorbents for heavy metals. *Water Research*, *33*(11), 2469–2479.
Berger, J., Reist, M., Mayer, J., Felt, O., Peppas, N., & Gurny, R. (2004). Structure and interactions in covalently and ionically crosslinked chitosan hydrogels for biomedical applications. *European Journal of Pharmaceutics and Biopharmaceutics*, *57*(1), 19–34.
Bessbousse, H., Rhlalou, T., Verchère, J. F., & Lebrun, L. (2008). Removal of heavy metal ions from aqueous solutions by filtration with a novel complexing membrane containing poly (ethyleneimine) in a poly (vinyl alcohol) matrix. *Journal of Membrane Science*, *307*(2), 249–259.
Bogert, M. T., & Renshaw, R. R. (1908). 4-amino-0-phthalic acid and some of its derivatives. 1. *Journal of the American Chemical Society*, *30*(7), 1135–1144.
Chen, A. H., Liu, S. C., & Chen, C. Y. (2008). Comparative adsorption of Cu (II), Zn (II), and Pb (II) ions in aqueous solution on the crosslinked chitosan with epichlorohydrin. *Journal of Hazardous Materials*, *154*(1–3), 184–191.
Cheung, W., Ng, J., & Mckay, G. (2003). Kinetic analysis of the sorption of copper (II) ions on chitosan. *Journal of Chemical Technology & Biotechnology*, *78*(5), 562–571.
Crini, G. (2006). Non-conventional low-cost adsorbents for dye removal: a review. *Bioresource Technology*, *97*(9), 1061–1085.
Deans, J. R., & Dixon, B. G. (1992). Uptake of Pb2+ and Cu2+ by novel biopolymers. *Water Research*, *26*(4), 469–472.
Desai, K., Kit, K., Li, J., Michael Davidson, P., Zivanovic, S., & Meyer, H. (2009). Nanofibrous chitosan non-wovens for filtration applications. *Polymer*, *50*(15), 3661–3669.
Gerente, C., Lee, V., Cloirec, P. L., & McKay, G. (2007). Application of chitosan for the removal of metals from wastewaters by adsorption—mechanisms and models review. *Critical Reviews in Environmental Science and Technology*, *37*(1), 41–127.
Grosse, D. (1986). Review of alternative treatment processes for metal bearing hazardous waste streams. *Journal of Air Pollution and Control Association (United States)*, *36*(5).
Hergenrother, P. M. (2003). The use, design, synthesis, and properties of high performance/high temperature polymers: an overview. *High Performance Polymers*, *15*(1), 3.
Hsien, T. Y., & Rorrer, G. L. (1995). Effects of acylation and crosslinking on the material properties and cadmium ion adsorption capacity of porous chitosan beads. *Separation Science and Technology*, *30*(12), 2455–2475.
Hu, Y. L., Lu, M., Liu, X. B., Zhang, S. B., Ji, Z. H., & Lu, T. T. (2010). An inexpensive and efficient synthetic method for the preparation of pyromellitic dianhydride promoted by ionic liquid. *ARKIVOC*, *9*, 63–74.
Jan iauskait, U., & Makuška, R. (2008). Polyelectrolytes from natural building blocks: synthesis and properties of chitosan-o-dextran graft copolymers. *chemija*, *19*(2), 35–42.
Kandile, N., Mohamed, M., Zaky, H., Nasr, A., & Abdel-Bary, E. (2009). Synthesis and properties of chitosan hydrogels modified with heterocycles. *Carbohydrate Polymers*, *75*(4), 580–585.
Kasaai, M. R., Arul, J., & Charlet, G. (2000). Intrinsic viscosity–molecular weight relationship for chitosan. *Journal of Polymer Science. Part B: Polymer Physics*, *38*(19), 2591–2598.
Kolhe, P., & Kannan, R. M. (2003). Improvement in ductility of chitosan through blending and copolymerization with PEG: FTIR investigation of molecular interactions. *Biomacromolecules*, *4*(1), 173–180.
Kumar, M. N. V. R., Muzzarelli, R., Muzzarelli, C., Sashiwa, H., & Domb, A. (2004). Chitosan chemistry and pharmaceutical perspectives. *Chemical Reviews*, *104*(12), 6017–6084.
Kurita, K., Kaji, Y., Mori, T., & Nishiyama, Y. (2000). Enzymatic degradation of [beta]-chitin: susceptibility and the influence of deacetylation. *Carbohydrate Polymers*, *42*(1), 19–21.
Lagergren, S. (1898). Zur theorie der sogenannten adsorption geloster stoffe. 591. Kungliga Svenska Vetenskapsakademiens. *Handlingar*, *24*(4), 1–39.
Langmuir, I. (1918). The adsorption of gases on plane surfaces of glass, mica and platinum. *Journal of the American Chemical Society*, *40*(9), 1361–1403.
Lavrov, S., Ardashnikov, A. Y., Kardash, I. Y., & Pravednikov, A. (1977). Cyclization of aromatic poly (amic acids) to polyimides. Cyclization kinetics of a model compound of N-phenylphthalamic acid. *Polymer Science USSR*, *19*(5), 1212–1219.
Lin, W. J., Chen, T. D., & Liu, C. W. (2009). Synthesis and characterization of lactobionic acid grafted pegylated chitosan and nanoparticle complex application. *Polymer*, *50*(17), 4166–4174.
Liu, F., Zhang, G., Meng, Q., & Zhang, H. (2008). Performance of nanofiltration and reverse osmosis membranes in metal effluent treatment. *Chinese Journal of Chemical Engineering*, *16*(3), 441–445.
Majumdar, A., & Biswas, M. (1990). Thermal stability, dielectric and conductivity characteristics of 9, 10-anthracene-diol-anhydride polycondensates. *Polymer Bulletin*, *24*(5), 565–572.
McKay, G., El Geundi, M., & Nassar, M. (1987). Equilibrium studies during the removal of dyestuffs from aqueous solutions using bagasse pith. *Water Research*, *21*(12), 1513–1520.
Metcalf, L., Eddy, H. P., & Tchobanoglous, G. (1991). *Wastewater engineering: Treatment, disposal, reuse*. New York: McGraw-Hill.
Meunier, N., Drogui, P., Montane, C., Hausler, R., Mercier, G., & Blais, J. F. (2006). Comparison between electrocoagulation and chemical precipitation for met-

als removal from acidic soil leachate. *Journal of Hazardous Materials*, *137*(1), 581–590.
Mittal, K., & Ghosh, M. K. (1996). *Polyimides fundamentals and applications*. P.O. Box 5005, Monticello, NY 12701-5185, USA: Marcell Dekker, Inc., 912 p.
Mittal, K.L. (2009). Polyimides and other high temperature polymers: Synthesis, characterization, and applications. Vsp.
Monteiro, O. A. C., Jr., & Airoldi, C. (1999). Some studies of crosslinking chitosan–glutaraldehyde interaction in a homogeneous system. *International Journal of Biological Macromolecules*, *26*(2–3), 119–128.
Monteiro, O. A. C. (1999). Some thermodynamic data on copper–chitin and copper–chitosan biopolymer interactions. *Journal of Colloid and Interface Science*, *212*(2), 212–219.
Ng, J., Cheung, W., & McKay, G. (2002). Equilibrium studies of the sorption of Cu (II) ions onto chitosan. *Journal of Colloid and Interface Science*, *255*(1), 64–74.
Nunthanid, J., Puttipipatkhachorn, S., Yamamoto, K., & Peck, G. E. (2001). Physical properties and molecular behavior of chitosan films. *Drug Development and Industrial Pharmacy*, *27*(2), 143–157.
Ofomaja, A., Naidoo, E., & Modise, S. (2010). Kinetic and pseudo-second-order modeling of lead biosorption onto pine cone powder. *Industrial & Engineering Chemistry Research*, *49*(6), 2562–2572.
Repo, E., Warchol, J. K., Kurniawan, T. A., & Sillanpää, M. E. T. (2010). Adsorption of Co (II) and Ni (II) by EDTA-and/or DTPA-modified chitosan: Kinetic and equilibrium modeling. *Chemical Engineering Journal*, *161*(1–2), 73–82.
Shantha, K. L., & Harding, D. R. K. (2002). Synthesis and characterisation of chemically modified chitosan microspheres. *Carbohydrate Polymers*, *48*(3), 247–253.
So, H. H., Cho, J. W., & Sahoo, N. G. (2007). Effect of carbon nanotubes on mechanical and electrical properties of polyimide/carbon nanotubes nanocomposites. *European Polymer Journal*, *43*(9), 3750–3756.
Sroog, C., Endrey, A., Abramo, S., Berr, C., Edwards, W., & Olivier, K. (1965). Aromatic polypyromellitimides from aromatic polyamic acids. *Journal of Polymer Science. Part A: General Papers*, *3*(4), 1373–1390.
Tian, S., & Xu, G. (1995). PMDA-ODA-PSX-DABSA copolymer for ionic conduction. *Polymer*, *36*(8), 1555–1558.
Tong, Y., Li, Y., Xie, F., & Ding, M. (2000). Preparation and characteristics of polyimide–TiO_2 nanocomposite film. *Polymer International*, *49*(11), 1543–1547.
Trimukhe, K., & Varma, A. (2008). Complexation of heavy metals by crosslinked chitin and its deacetylated derivatives. *Carbohydrate Polymers*, *71*(1), 66–73.
Ucer, A., Uyanik, A., & Aygun, S. (2006). Adsorption of Cu (II), Cd (II), Zn (II), Mn (II) and Fe (III) ions by tannic acid immobilised activated carbon. *Separation and Purification Technology*, *47*(3), 113–118.
Varma, A., Deshpande, S., & Kennedy, J. (2004). Metal complexation by chitosan and its derivatives: a review. *Carbohydrate Polymers*, *55*(1), 77–93.
Wan Ngah, W., Endud, C., & Mayanar, R. (2002). Removal of copper (II) ions from aqueous solution onto chitosan and cross-linked chitosan beads. *Reactive and Functional Polymers*, *50*(2), 181–190.
Wu, F. C, Tseng, R. L., & Juang, R. S. (2001). Enhanced abilities of highly swollen chitosan beads for color removal and tyrosinase immobilization. *Journal of Hazardous Materials*, *81*(1–2), 167–177.